Ethiopian Journal of Water Science and Technology (EJWST)

DOI: https://doi.org/10.59122/17519g6

Vol. 6 , 2023, Pages: 75~108 ISSN(Print): 2220-7643

Evaluation of meteorological drought and its impact on cereal yield over Afar region, northeast Ethiopia

Tadele Badebo[1, 2], Abebe Kebede[2], and Thomas T. Minda[2,*]

[1] Ethiopian Meteorology Institute, Addis Ababa, Ethiopia
[2] Faculty Meteorology and Hydrology, Water Technology Institute, Arba Minch University, Ethiopia
[*] Corresponding author at Arba Minch University, P.O.Box 21. E-mail: thomas.torora@amu.edu.et; tororathomas@yahoo.com (T.T. Minda)

Abstract

Drought is a natural disaster resulting from an extended period of insufficient precipitation, leading to an inability to meet the needs of humans, livestock, and the environment. In Ethiopia, frequent and severe droughts increasingly affect the socio-economic and environmental sectors. This study evaluates the current and future projected meteorological drought and its impact on major cereal crops yield over the Afar region in northeast Ethiopia. We used surface stations, satellite climate estimates, downscaled atmospheric reanalysis, and regional climate model datasets. We evaluated the occurrence of drought using the Standardized Precipitation Index (SPI) and Standardized Precipitation and Evapotranspiration Index (SPEI) calculated at 3-month and 12-month time scales. The drought vs. regional cereal yield is correlated to explain yield variability in the region. Results showed that more intense droughts were analyzed in 1984, 1985, 2002, 2008, 2009, 2010, 2015, and 2016. Among these years, 1984, 2002, 2008, 2009, and 2015 were the driest years across all locations in the study area. The regression of SPI and SPEI with yield showed that the indices significantly explained (r^2 = 0.56 for SPI and 0.18 for SPEI) the observed yield variation. Spatially, more intense drought prevails over the northern, northwestern, and southwestern parts of Afar, where these parts are more prone to severe drought. The projected drought pattern showed increases in the intensity and frequency of drought in the middle and end of the century. The findings of this study are helpful for stakeholders working on drought mitigation in the region.

Keywords: climate change, crop yield, drought projection, meteorological drought.

Received: 15 Apr 2023; accepted 10 May 2023 Published: December, 2023

1 INTRODUCTION

Drought is a natural hazard and recurrent climatic event caused by a deficiency of precipitation with prolonged periods of high temperature (WMO, 2006) Drought occurs in nearly all parts of the world and all economic systems with varying frequency and severity (Wilhite & Glantz, 1985). Its magnitude, duration, and frequency govern the impact of drought. Drought magnitude refers to the amount of rainfall deficit at a particular place and specific time, whereas duration refers to the length of time a drought event stays (Saravi et al., 2009). Drought intensity is the ratio of drought magnitude to duration, which indicates the level of severity or degree of deficit. Meanwhile, drought frequency is the number of drought events in a given time and indicates how frequent drought is in a specific area (Mohammed et al., 2018).

The ongoing climate change has a significant impact on drought. Drought's intensity and duration increase when temperature rises because a higher temperature causes more evaporation and surface drying. For example, the earth's surface air temperature over global land area has increased by about 1.7% since 1970 (Dai, 2011). Studies showed that the global arid zone is very dry, increasing from 10–15% in the early 1970s to 30% in 2002 (Dai, 2011; Feng & Zhang, 2015). Drought has increased worldwide over the 20th century (Aiguo et al., 2004; Trenberth et al., 2014). Studies revealed that drought had become more frequent and intense since 1970, affecting African countries more, with most of this drought caused recently. For example, the frequency and intensity of numerous extreme, multi-year droughts increased every century, with the longest and most intense drought recently occurring in the Sahel and equatorial countries of East Africa (Masih et al., 2014). For instance, estimates of the impact of drought indicate that between 1900 and 2013, about 291 droughts were recorded in Africa, causing enormous losses to humanity, killing almost a million people, and causing an economic loss of over 3,000 million dollars (Masih et al., 2014). Many scholars have investigated future drought changes using projected climate datasets (Teshome & Zhang, 2019, Haile et al., 2020). Haile et al. (2020) indicated a decreasing rainfall trend for the June-September primary rainy season and increased variability for the February to May rainy season over Ethiopia. The projected rainfall extremes of very wet days and the number of heavy rainfall days showed a decreasing trend (Teshome & Zhang, 2019). Both daily maximum and minimum temperatures showed a significantly increasing trend. Accordingly, in Eastern Africa, drought conditions are likely to increase by 16%, 36%, and 54% by the end of the century under low, medium, and business-as-usual emission scenarios, respectively (Haile et al., 2020).

In Ethiopia, more severe and frequent droughts are increasingly affecting the socio-economic sector, particularly the agricultural sector. Agriculture makes up the majority of the country's economy, as more than 95% of the crop production is based on rain-fed agriculture (Minda et al., 2018). Rainfall dependency on the agricultural sector results in a continuous problem with food security (WFP, 2014). The large majority of the people living in Afar regional state of Ethiopia are pastoralists, deriving their income and subsistence mainly from rearing livestock. According to Famine Early Warning System Network (FEWSNET) report, the humanitarian situation has changed dramatically due to the 2015/2016 drought since the beginning of 2017 in Somali and Afar regions. Thus, the 2015/2016 drought is resulted in large livestock losses and caused severe food insecurity in the pastoral areas of Ethiopia (FEWSNET, 2016).

During drought periods, for example, cereal crop prices increase due to demand-supply imbalance, while livestock prices decrease due to poor body condition and feed scarcity. Studies indicated that the price of main cereal crops increased at the national level during the 1997/98 drought period. Prices of sorghum, wheat, maize, and Teff were 13%, 38%, and 47% higher in the third quarter of 1998 compared to the first quarter of 1997 period (Bachewe et al., 2017). In the 2015 drought period, the price of oxen in January 2017 was 13% lower than that of January 2014, and sheep in January 2017 was 9.4% lower than in January 2014 (Bachewe et al., 2017). According to Ethiopia's Central Statistical Agency (CSA), following the 2015 drought, grain crop production decreased by 13.3% and 15.4% in Afar and Somali pastoralist regions, respectively (CSA, 2018).

Among the numerous drought indices, the most commonly used indices are the Standardized Precipitation Index (SPI) (McKee et al., 1993) and the Standardized Precipitation and Evapotranspiration Index (SPEI) (Vicente-Serrano et al., 2010). The SPI has been increasingly used during the last two decades because of its solid theoretical development, robustness, and versatility in drought analysis and quantification (Quiring, 2009). The SPEI was first proposed as an improved drought index that is especially suited for studies of the effect of global warming on drought severity. Although the steps calculating the SPEI and SPI are similar, the SPEI is based on a climatic water balance that is adjusted using a three-parameter log-logistic distribution (Vicente-Serrano et al., 2010). It is also noted that many researchers have used SPI and SPEI simultaneously to study the impact of drought on crop performance as indicators of drought (Begna, 2020; Mohammed et al., 2022). Drought is the most complicated and least understood of all natural disasters. Its complex and widespread nature makes it difficult to define its beginning and end (Gerber & Mirzabaev, 2019). The application of SPI and SPEI is very important to evaluate drought

indices as tools for monitoring, evaluating and testing their ability to explain the variance of crop yield during the growing season. Moreover, it is important that which drought index, SPI or SPEI that more explaining the variance of crop yield over the study area. Therefore, this study aims to assess the past and future variations of drought characteristics and their impact on cereal crop productivity using SPI and SPEI drought indices in Afar region, Ethiopia. Accordingly, we formulated the following research questions to be addressed in this study:

i. How is the spatiotemporal variation of drought characterized during the last 40 years (1981-2020) in the Afar region?
ii. What are the expected changes in drought in the coming decades compared to the base period?
iii. What is the association between drought and rain-fed cereal crop productivity in the study area?

2 MATERIALS AND METHODS

2.1 Description of the study area

The Afar region is located northeast of Ethiopia (Figure 1). The region is geographically located between 8° 51' and 14° 34' N and 39° 47' and 42° 24' E, and has an area of about 94,760 km^2 (Wakie et al., 2014). According to the Ethiopian Economic Association report, the region is divided into five administrative zones (EEA, 2021).

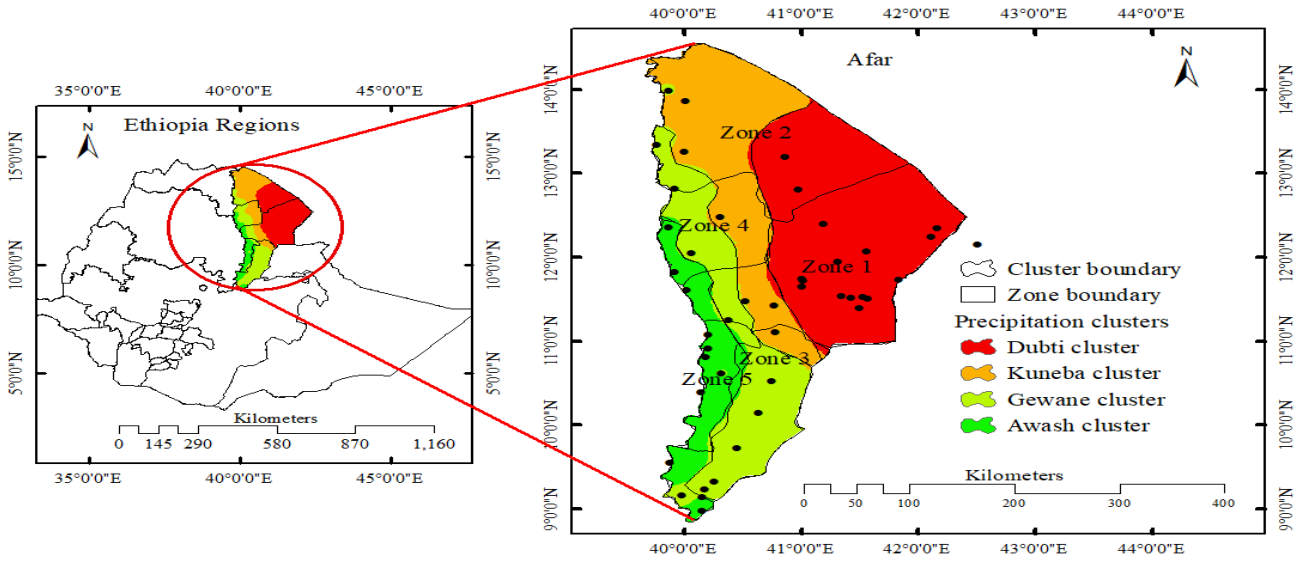

Figure 1| Study area map: spatial distribution of 44 meteorological stations indicated by circled dots that were used in this study. The rainfall stations were first categorized into clusters based on rainfall spatial coherence and clustered into four, namely the Dubti cluster, Kuneba cluster, Gewane cluster, and Awash cluster, using the K-mean clustering approach. Additional data is provided in the attached supplementary materials.

The rainfall of the study area is bimodal, with two wet seasons. The first rainy season extents from February to May (FMAM), known as Belg, while the second and main rain season spans from June to September (JJAS), known as Kiremt, as per the Ethiopian Meteorology Institute (EMI) classification (Aytenfisu, 2024). The Belg rain peaks in April while the Kiremt rains in August (Gummadi et al., 2018). The mean annual rainfall is 740.5 mm, while the mean annual, daily minimum, and maximum temperatures are 28.3, 19.8, and 37.3 ℃, respectively (Wakie et al., 2014; Gummadi et al., 2018).

The livelihood of the Afar people is predominantly pastoralism. However, due to recurrent drought, which resulted in a decreasing number of livestock, the pastoral mode of production has been challenged occasionally, and the pastoral households have entered into alternative livelihoods such as agro-pastoralism (Diriba, 2020). According to the CSA report, rain-fed agriculture has been practiced in Afar, and at the moment, a significant portion of households are engaged in crop production in the region. Among cereal crops, Teff, barley, wheat, maize, and sorghum are the most commonly grown crops grown in the region (CSA, 2021).

2.2 Data

We used daily rainfall, maximum, and minimum temperature data from 44 weather stations (> 70% of the total available stations in the Afar region) obtained from the EMI for the period 1981 to 2020 (Figure 1). Since there are gaps in the gauged data, other data sources are utilized to fill the gaps. The missed rainfall data is filled from the Climate Hazards Group Infrared Precipitation (CHIRP). The CHIRP dataset has been used in drought monitoring and evaluations (Tuo et al., 2016; Kebede et al., 2020). The detailed description of the data was provided by Funk et al., (2015) and Dinku et al., (2018). To fill in the daily maximum and minimum temperature data, we used the European Center for Medium-range Weather Forecast's (ECMWF) fifth-generation Atmospheric Reanalysis downscaled at the spatial resolution of 10×10 km^2 (AgERA5). The performance of the data is evaluated over East African countries (Gleixner et al., 2020).

2.2.1 CMIP5 climate projections

The Coupled Model Inter comparison Project phase 5 (CMIP5) dataset provide a quantitative assessment of future drought projection. From the CMIP5 model groups, we used five Regional Climate Models (RCMs) dynamically downscaled for the Coordinated Regional Downscaling Experiments (CORDEX) for the Africa domain. Several scholars in Ethiopia have evaluated these models, and their findings indicate well-simulated rainfall and temperature in Ethiopia (Worku et al., 2018). Details of the models are presented in Table 1.

Table 1| Descriptions of RCMs utilized in this study and their deriving sources.

Description of RCM	**Driving sources**	**Country**	**RCM**
Regional Atmospheric Climate Model version 2.2	EARTH	The Netherlands	RACMOO22T
Swedish Meteorological and Hydrological Institute (SMHI), The Rossby Centre Regional Climate model version 4	CNRM-CERFACS-	Sweden	SMHI-RCA4
Consortium for Small-scale Modeling (COSMO) Climate Limited Area Modelling Community (CLMcom)	CNRM-CERFACS-CNRM-CM5	USA	CCLM4-8-17
Max Planck Institute for Meteorology-Climate Service Center (MPI-CSC), Regional Model	MPI-*M*-MPI-ESM-LR	Germany	REMO2009
Swedish Meteorological and Hydrological Institute (SMHI), version 4	CCCma-CanESM2	Sweden	CanRCA4

The average drought changes concerning the reference period (1981-2005) are computed for the near future (2006-2040), mid-century (2041-2070), and end-century (2071-2100) future projected periods. The three-slice sub-division investigates the possibility of significant variations in drought conditions as applied in literature (Park et al., 2015; Haile et al., 2020). Two Representative Concentration Pathways (RCP4.5 and RCP8.5) emission forcing was selected. These pathways are representative of medium emission (RCP4.5) and higher emission (RCP8.5) scenarios described by Riahi et al., (2011) and Thomson et al., 2011).

2.2.2 Bias correction

The power transformation (PT) method corrects the precipitation bias. This method is often used to correct precipitation data from climate models. It was implemented in Ethiopia and achieved high-quality performance (Tumsa, 2022).

$$P^{cor}\,hst, m, d = P^{b}_{hst,m,d} * [\frac{u(P_{obs,m})}{u(P_{hst,m})}] \quad (1)$$

Where $P^{cor}\,hst, m, d$ denote the corrected precipitation on the d^{th} day of the m^{th} month and $P_{hst,m,d}$ denote the simulated precipitation outputs during the relevant period, the subscripts d and m are specific days and months, respectively, and u denotes the mean value, b is a random constant number called correction factor.

The maximum and minimum temperatures are corrected using the Linear scaling (LS) bias correction method. The scaling approach is mainly linear and adjusts the climatic factors based on the differences between observed and model output explained by Zollo et al., (2014) and Crochemore et al., (2016).

$$T^{cor}\,hst, m, d = T_{hst,m,d} + [u(T_{obs,m}) - u(T_{hst,m})] \quad (2)$$

Where $T^{cor}\,hst, m, d$ denote the corrected temperature on the d^{th} day of the m^{th} month, and $T_{hst,m,d}$ denote the simulated temperature outputs during the relevant period, the subscripts d and m are specific days and months, respectively, and μ denotes the mean value.

2.2.3 Data clustering

The annual mean precipitation dataset from the 44 stations clusters similar rainfall regimes using a centroid-based approach known as the K-means clustering method. The k-mean algorithm is the most widely used iterative algorithm in data clustering, which iterates to determine the optimal value of the centroid. In the k-mean approach, the ideal numbers of clusters are calculated using a graphical technique called the elbow method noted by Nanjundan et al., (2019) and Umargono et al., (2020). The algorithm's performance improves with a smaller inertia value.

$$J = \sum_{i=1}^{m}\sum_{k=1}^{K} Wik||Xi - \mu k||^2 \quad (3)$$

Where $|Xi - Vj|$ is the Euclidean distance between xi and Vj, k is the number of data points at the i^{th} cluster, m is the number of cluster centers, Xi is the set of data points, and μk is the set of centers, respectively. $Wik = 1$ for data point Xi if it belongs to cluster K; otherwise, $Wik = 0$ and μk are the centroid of Xi's cluster, respectively.

$$Wik = \begin{cases} 1 \text{ if } k = \text{argmin}, \ ||Xi - \mu k||^2 \\ 0 \qquad\qquad \text{otherwise} \end{cases} \quad (4)$$

In other words, assign the data points Xi to the closest cluster judged by its sum of squared distance from the cluster's centroid.

$$\mu k = \frac{\sum_{i=1}^{m} WikXi}{\sum_{i=1}^{m} Wik} \quad (5)$$

2.2.4 Model performance evaluation

In this study, three statistical parameters are implemented to evaluate the performance of regional climate models performance whether they are reproducing the observed past climate variables over the period of 1981 to 2005. The statistical metrics in this study are comprising Pearson Correlation, Mean Root Square

error (MRSE) and Bias (BIAS), respectively. The RMSE measures the absolute mean difference between the observed and simulated dataset, where the value of RMSE is closer to zero, it is well scored (Chai et al., 2014). The Pearson correlation measures the linear relationship between two variables, which is used to evaluate the performance of RCMs in simulating the local climatic variables. Boslaugh (2012) states that the correlation coefficient (r) ranges from -1 to +1 when the value of r is 0.1 is taken as small, 0.3 is taken as medium, and 0.5 is taken as high model performance. The Pearson correlation coefficient is computed as:

$$r = \frac{\sum_{i=1}^{n}(O-\overline{O})(M-\overline{M})}{\sqrt{\sum_{i=1}^{n}(O-\bar{O})^2} * \sqrt{\sum_{i=1}^{n}(M-\bar{M})^2}} \quad (6)$$

Where r is the correlation coefficient, O is observed rainfall, $\overline{O}$ is observed rainfall, M is model rainfall, and $\overline{M}$ is the mean of model rainfall. The Bias measures the systematic error between the observed and simulated climate variables, and when the value close to zero, indicating good performance of the model, while values away from zero, the models deviate from the observations. When the value is negative, indicate the models are underestimating while the value is positive, the models are overestimating (Florida, 2021).

$$BIAS = \frac{\sum_{i=1}^{N}(S_i - O_i)}{\sum_{i=1}^{N} O_i} \quad (7)$$

$$RMSE = \sqrt{\sum_{i=1}^{n} \frac{(S_i - O_i)^2}{N}} \quad (8)$$

Where S and O are the simulated and observed values, respectively, while i refers to the simulated and observed pairs and N is the total number of such pairs.

2.2.5 Crop yield data

Drought is a major factor influencing cereal crop production and productivity in most of the rain-cultivated areas across Ethiopia. So, it is interesting to analyze how current drought indices are associated with the cereal yields in the region. As a result, the average cereal yields provided by the CSA, (2019) for 1994-2019 period, and reported as a growing period yield sum for entire Afar region (CSA, 1996). As the Kiremt (June-September) cropping season is the main cereal crop production season, we focused on this cropping

season in our study. The cereal crops we considered are mainly the total sum of maize, teff, and sorghum, as these are staple foods of the region.

2.3 Methods

In this study, we implemented the SPI and SPEI meteorological drought indices to evaluate the characteristics of drought and its impact on crop yield. The indices are calculated using the Climate Data Tool (CDT). As mentioned by Nsengiyumva et al., (2021) and Dinku et al., (2022), CDT is an open-source, R-based software with an easy-to-use graphical user interface used by over 20 countries.

2.3.1 Standardized precipitation index

To assess long-term and medium-term drought occurrences, the SPI value and its probability density function of the gamma distribution are calculated as:

$$g(x) = \frac{1}{\beta^{\alpha}\Gamma(\alpha)} x^{\alpha-1} e^{-\frac{x}{\beta}}, \text{for } x > 0 \quad (9)$$

Where $\alpha > 0$ is a shape parameter, $\beta > 0$ is a scale parameter, $x > 0$ is the amount of precipitation, and (α) is the gamma function. The probability that the random variable x is less than x_0 can be computed for the precipitation x_0 in a certain year:

$$F(x < x_0) = \int_0^{\infty} f(x)\, dx \quad (10)$$

$$F(x = 0) = \frac{m}{n} \quad (11)$$

Where m is the number of samples with precipitation of 0 and n is the total number of samples. To normal standardized processing of Γ probability distribution, we have substituted the result of probability value into the normalized normal distribution function:

$$F(x < x_0 = \frac{1}{\sqrt{2\pi}} \int_0^{\infty} e^{-x^2/2} dx \quad (12)$$

The SPI can easily be obtained as the standardized values of F(x) and calculated as:

$$SPI = S \frac{t-(c_2 t + c_1)+c_0}{[(d_3 t + d_2)t + d_1]t+1} \quad (13)$$

Where $t = \sqrt{ln\frac{1}{F^2}}$ and $c_0 = 2.515517, c_1 = 0.802853, c_2 = 0.010328, d_1 = 1.432788$

$d_2 = 0.189269\ and\ d_3 = 0.001308$, respectively. Where S is the probability density plus or minus coefficient. If F > 0.5, then $S = 1$, if F ≤ 0.5, then $S = -1$.

2.3.2 Standardized precipitation and evapotranspiration index

SPEI is calculated similarly based on the difference between potential Evapotranspiration (PET) and Precipitation (P). This study used the modified Hargreaves method based on only observed temperature values (Hargreaves & Allen, 2003). The difference between P and PET is computed as follows

$$D_i = P_i - \text{PET}_i \quad (14)$$

$$\text{PET} = 0.0023(Tmax - Tmin)^{0.5} * (Tmean + 17.8) * Ra \quad (15)$$

Where PET is potential evapotranspiration (mm day^{-1}), $Tmax$, $Tmin$, and $Tmean$ are maximum, minimum, and mean air temperature (^{o}C).

R_a is extraterrestrial radiation given in (mm day^{-1}), computed from latitude and the day of the year

$$\text{Ra} = \frac{1440}{\pi}(\text{Gsc. Dr})[\varphi \text{sign}(\varphi)\sin(\sigma) + \cos(\varphi)\cos(\sigma)\sin(\varphi s)] \quad (16)$$

$Gsc = 0.0820 \text{MJ m}^{-2}$, is solar constant

$Dr = 1 + 0.022\cos\left[\frac{2\pi(JD)}{365}\right]$ is the inverse relative distance from the Earth to the Sun (17)

$JD\ is\ a\ day\ of\ the\ year$

$\varphi s = arcos[-\tan(\varphi)\tan(\sigma)]$ is the sunset hour angle (rad) (18)

$\sigma = 0.409\sin(2\pi\frac{JD}{365} - 1.39)$, is the solar declination (rad) (19)

φ is the latitude of the location

$\frac{MJ}{m^2 d}$, can be converted to mm/d: as $\frac{mm}{d} = \frac{1}{2.43} * \frac{\frac{MJ}{m^2}}{d}$

Di is quantified at different time scales using the same procedure as SPI. The difference between the specific months j and year i depends on the selected time scale k. For example, the accumulated difference for j month in a given year i with k-month time scale is calculated using the formula:

$$X_{i,j}^{k} = \sum_{I=k+i,\ k+j}^{k} D_{i-I,j} + \sum_{I=1}^{j} D_{i,j}\ ,\ \text{if j < k} \quad (20)$$

$$X_{i,j}^{k} = \sum_{I=j-k+j}^{k} D_{i,j,}\ \text{if j} \geq \text{k} \quad (21)$$

Where $D_{i,j}$ is the difference between P and PET of the first month of the year i, given in mm. The three parameters of the log-logistics probability density function are used to fit the data series and expressed as follows:

$$f(X) = \left(\frac{\beta}{\alpha}\right)\left(\frac{x-\gamma}{\alpha}\right)^{\beta-1}\left[1+\left(\frac{x-\gamma}{\alpha}\right)^{\beta}\right]^{-2} \quad (22)$$

Where α, β, and γ represent the scale, shape, and location parameters, respectively, that are estimated from the data series Di. Parameters of the log-logistic distribution obtained by the L-moment procedure that is the most robust and easy approach Reath et al., (2018).

$$\beta = \frac{2w1-w0}{6w1-w0-6w2} \quad (23)$$

$$\alpha = \frac{(w0-2w1)\beta}{\left(1+\frac{1}{\beta}\right)\left(1-\frac{1}{\beta}\right)} \quad (24)$$

$$\gamma = w0 - \alpha\Gamma\left(1+\frac{1}{\beta}\right)\Gamma \quad (25)$$

Thus, the cumulative distribution function of a given time scale is computed as follows:

$$F(\text{x}) = \left[1+\left(\frac{x-\gamma}{\alpha}\right)^{\beta}\right]^{-1} \quad (26)$$

The SPEI can easily be obtained as the standardized values of F(x) and calculated as:

$$\text{SPEI} = \text{w} - \frac{\text{C}_0+\text{C}_1\text{W}+\text{C}_2\text{W}^2}{1+\text{d}_1\text{w}+\text{d}_2\text{w}^2+\text{d}_3\text{w}^3} \quad (27)$$

$$\text{w} = \sqrt{-2\ln(\text{P})}$$

$\text{C}_0 = 2.51517, \text{C}_1 = 0.802853,\ \ \text{C}_2 = 0.0103288,\ \ \text{d}_1 = 1.432788,\ \ \text{d}_2 = 0.189269,$ and $\text{d}_3 = 0.001308$ and P is the probability of exceeding a determined D_i value, $\text{p} = 1 - \text{F}(x)$ if p > 0.5, then p is replaced by $1 - \text{p}$ and the sign of the resultant SPEI is reversed. Guttman, (1999)

Guttman, (1999) and Vicente-Serrano et al. (2010) categorized the drought characteristics into different severity levels, as indicated in Table 2. The authors also defined the drought event criteria for any time scale. The number of months in which SPI/SPEI values are consecutively ≤ -1 is considered a drought incident and determines the duration of the incident. The drought event ends when the SPI/SPEI becomes positive. Therefore, each drought event has a duration defined by its beginning and end and an intensity for each month the event continues. The positive sum of the SPI/SPEI within a drought event is known as drought magnitude (WMO, 1987).

Table 2| SPI and SPEI drought categories defined by drought severity regimes

Anomaly	Range of SPI/ SPEI values (d_value)	drought severity regime
Positive	2.0 < d_value <= MAX	Extremely wet
	1.5 < d_value < = 2.0	Very wet
	1.0 < d_value <= 1.5	Moderately wet
None	-1.0 < d_value <= 1.0	Normal precipitation
Negative	-1.5 < d_value <= -1.0	Moderately dry
	-2.0 < d_value <= -1.5	Very dry
	MIN <= d_value <= -2.0	Extremely dry

The SPI is considered to enumerate the rainfall deficit for multiple timescales. These time scales reveal the impression of drought on the accessibility of the different water resources. We selected the 3-month and 12-month time scales of SPI and SPEI to evaluate past and future drought occurrence for the following reasons. The 3-month SPI/SPEI reveals medium-term moisture conditions of the current month and the past two months, providing a seasonal rainfall estimation for seasonal crop production. The 12-month period reflects the long-term rainfall patterns that compare the rainfall for 12 consecutive months with that recorded in the same 12 consecutive months in all previous years without missing data (WMO, 1987).

2.3.3 Drought trend

The Mann-Kendal (MK) test is used to perceive statistically significant decreasing or increasing trends in long-term temporal datasets by Mann, (1945) and (Wang & Vrijling, (2005). The MK trend test is based on two hypotheses: one is null (Ho), and the other is the alternative (H1) hypothesis. The Ho expresses the existence of no trend, while H1 elucidates a significant rising or declining trend in the temporal drought

pattern. Based on the 5% significant level, if the p-value is < 0.05, the alternative hypotheses are accepted, which signifies the presence of a trend in the data. If the p-value is > 0.05, the null hypothesis will be accepted, which denotes the absence of a trend in the data. The following equations provide the computational steps for the trend.

$$S = \sum_{i=1}^{n-1} \sum_{j=i+1}^{n} \sin(T_j - T_i) \quad (28)$$

Where T_j and T_i are the monthly, seasonal, and annual values in years' j and i, j > i respectively, n is the number of data points. Assuming $(T_j - T_i) = \theta$, the value of sign (θ) is computed as follows:

$$\sin(T_j - T_i) = \begin{cases} 1; & if \quad Tj - Ti > 0 \\ 0; & if \quad Tj - Ti = 0 \\ -1; & if \quad Tj - Ti < 0 \end{cases} \quad (29)$$

A positive value of S indicates an increasing trend, whereas a negative value indicates a declining trend in the data. The magnitude of drought is evaluated by a simple non-parametric procedure using Sen's slope estimator developed by Sen (1968) and calculated as follows:

$$Q_i = \left(\frac{x_j - x_i}{j-1}\right) \quad (30)$$

Where i = 1 to n-1, j = 2 to n, $\mathbf{x_j}$ and $\mathbf{x_i}$ are data values at time j and i where (j > i), respectively. If there are n values of $\mathbf{x_j}$ in the time series, Sen's slope estimator will be N = n(n-2)/2. The Sen's slope estimator is the mean slope of N values; then, the Sen's slope is estimated as:

$$Q_{ij} = \begin{cases} \frac{x_j - x_i}{j-1}; & if\ n\ is\ odd \\ \frac{1}{2}\left(Q\frac{N}{2} + Q\left[\frac{N+2}{2}\right]\right); & if\ n\ is\ even \end{cases} \quad (31)$$

The positive value of $\mathbf{Q_{ij}}$ indicates an increasing trend, while the negative value of $\mathbf{Q_{ij}}$ shows a decreasing trend, where the units of Sen's slope ($\mathbf{Q_{ij}}$) is the slope per year in the temporal dataset.

The MK trend test is a nonparametric test widely used to detect significant trends in a set of time series data. However, researchers have shown that the original Mann-Kendall test did not consider serial correlation in a time series data set Hirsch, (1981) and Bari et al., (2016). Furthermore, in many real-world situations, observed data are autocorrelated, which can lead to misinterpretation of the results of trend estimates (Cox et al., 2013; Hamed & Rao, 1998). Consequently, Hamed & Rao, (1998) have developed a modified Mann-Kendall trend test that is based on the assumption that time series data are

serially correlated and therefore autocorrelation is addressed by a modified MK trend test. The modified MK trend test has been used by many researchers to eliminate the influence of serial correlation in the original MK trend test in time series trend detection studies Yue & Wang, (2015) and Patakamuri & Brien, (2021). In this study, we use the modified MK trend test developed by Hamed & Rao, (1998).

2.3.4 Drought and crop yield correlation

Climate variability seriously threatens the productivity of Ethiopia's food crops. Understanding the impact of extreme weather events on agricultural production is crucial for resilience to climate change and improving food security. To determine the context and magnitude of drought-induced yield fluctuations, it is necessary to eliminate or minimize the influence of non-climatic factors such as variety, management, and technology to eliminate biases arising from these trends. Crop yield anomalies are identified from declining time series using a linear regression method, and drought indices are linked to yield anomalies. Several researchers have used a linear regression model to modify yield trends and used the resulting anomalies to determine the effects of drought on crop yield by Lobell & Asner, (2003) and Potopova et al., (2016). A simple linear regression model is given as follows:

$$Y_t = \alpha + \beta * X_t \tag{32}$$

Where Y_t represents a yield anomaly at time t, α represents the constant, which is called the intercept of the regression model, $and\ \beta$ is a regression coefficient of the independent variable, which represents the gradient of the line and is referred to as the slope. X_t is an independent variable.

The association between de-trended yield and drought indices is explored through correlation analysis using a statistical package for social studies (SPSS). The correlation results provide initial information on the positive or negative associations, which helps to understand the regression results. Finally, a linear regression analysis of the de-trended yield and drought indices is performed to quantify the percentage response of determinant (r^2) of yield variations achieved jointly by SPI and SPEI at a 4-month time scale. The yield anomalies (Y_t) at time t are calculated as follows:

$$Y_t = \mathrm{y} - \mu \tag{33}$$

The crop data is regional yield data (quintal per hectare, qt/ha) for the entire Afar region for the Kiremt cropping season from 1994 to 2019. Since the climate of the study area is bimodal, FMAM and JJAS, the SPI and SPEI at a 4-month time scale are used to evaluate the impact of drought on crop yield.

2.3.5 Assessing drought characteristics

Drought characteristics can be expressed by these essential features such as duration, frequency, magnitude, intensity, severity, spatial-temporal room by Ettenmaier, (2005) and Alamgir et al., (2015). The duration, severity, intensity and frequency of the drought events were computed based on Table 2. The frequency of the drought is the number of months in which the SPI/SPEI value agrees as a set value in Table 2 and divided by the number of months in the whole sequence (Wang et al., 2014).

$$F = \frac{n}{N} * 100 \quad (34)$$

Where n is the number of months of drought events when the SPI/SPEI is less than - 1 that a drought index value agrees a set of drought criterion divided by the number of months in the whole series (N). The drought frequency (F) is used to assess the drought prevalence during the study period over the region. The drought duration is the length of drought period. Whereas the drought magnitude (M) is the cumulative sum of the drought index value based on the duration of the drought occurrence when the SPI/SPEI value is less than or equal to -1 and computed as:

$$M = \sum_{i\leq -1}^{D} SPI/SPEI \quad (35)$$

Similarly, the intensity of a drought (I) is the ratio of drought magnitude (M) to drought duration (D), respectively. Events that have a shorter duration and higher magnitude will have larger intensities.

$$I = \frac{M}{D} \quad (36)$$

Moreover, the inverse distance weighting approach is implemented to visualize and interpolate the spatial patter of drought characteristics with the support of ARC-GIS tool.

3 RESULTS

3.1 Temporal pattern of drought

Time series plots of drought indices are derived from station-wide and spatial averages of 44 meteorological stations' precipitation and temperature datasets for the 1981-2020 period. The average change in drought magnitude and frequency under global warming is investigated using five RCMs of daily precipitation and temperature datasets to understand how frequently the drought will likely occur. The drought characteristics, such as frequency and intensity, are used to evaluate the occurrence of drought over the study area using SPI and SPEI at 3-month and 12-month time scales. Furthermore, the drought

index for the crop growing season is calculated based on the seasonal classification of the study area, which mainly includes Belg and Kiremt crop growing seasons. Therefore, SPI and SPEI at a 4-month time scale are used to evaluate the impact of drought on crop yield.

Figure 2 depicts the spatially averaged time series plot of SPI and SPEI at 3- and 12-month time scales for the 1981-2020 period. The finding shows that severe drought prevailed in 1984, 1987, 1994, 1999, 2002, 2007, 2008, 2009, and 2015, whereas extreme drought prevailed in 2016. These years are considered the most intense drought episodes, with a severity scale of -1.50 to -5.35. 1984, 2008, 2009, and 2015 are considered the driest years across all locations. The drought intensity quantified by the SPEI 3-month and SPEI 12-month time scales were -1.36 and -1.47, with the extreme drought of -2.17 and -2.01; this extreme drought was quantified in 1984 and 2015, respectively. Whereas the drought intensity quantified by SPI 3-month and SPI 12-month time scales were -1.50 and -1.77 with extreme drought of -3.15 and -2.8, this extreme drought was evaluated for 1984 (Figure 2).

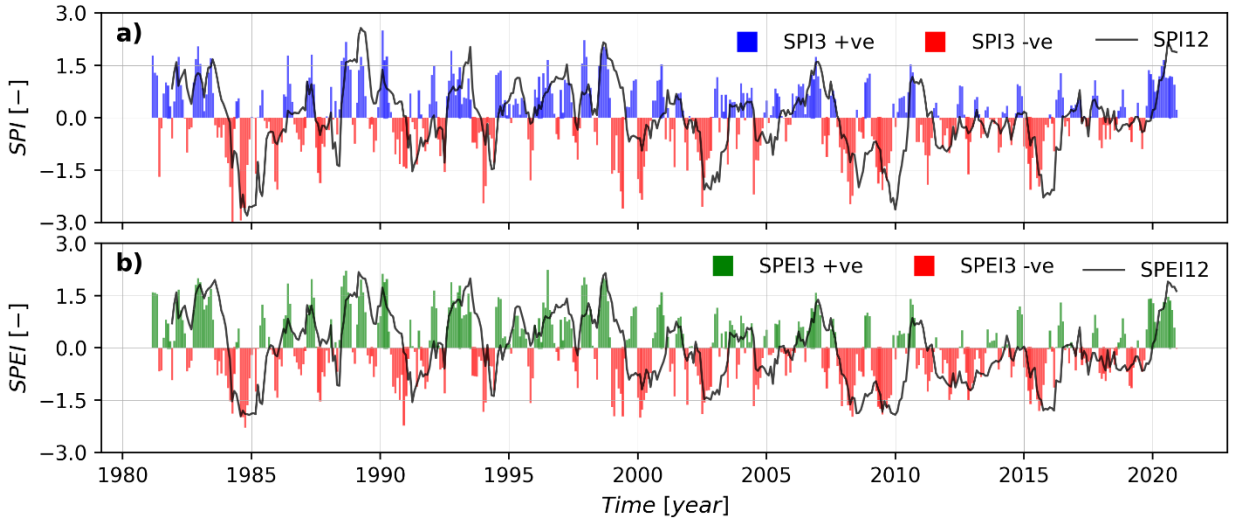

Figure 2| Spatial averaged time series plot for SPI (a) and SPEI (b) at a 3-month (bar-plots) and 12-month (line-plot) time scale. Blue (SPI) and green (SPEI) colors represent positive values, and red represents negative values.

The SPI and SPEI values at 3-month and 12-month time scales at cluster representative stations (Figure 1) are presented in Figure 3 and Figure 4. The results indicate the presence of severe to extreme drought conditions. For instance, extreme drought quantified by SPI 3-month time scale at Argoba (-4.49 for 2015), Dubti (-2.11 for 2015), Gewane (-4.03 for 2017) and Kuneba (-3.54 for 2015). At the same time,

extreme drought quantified by SPI-12-month time scale for the stations were -4.50, -2.98 -2.57, and -4.01, calculated for 2015, 1999, 1984, and 2015, respectively (Figure 3).

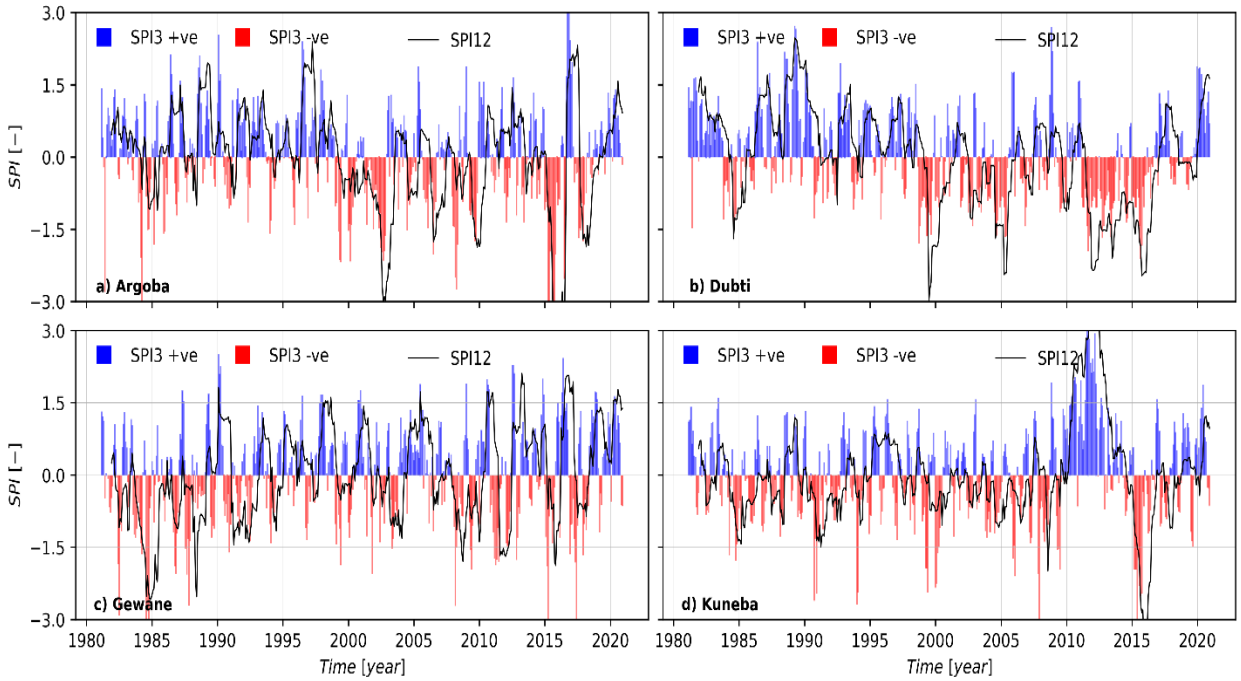

Figure 3| Time series plot for Argoba (a), Dubti (b), Gewane (c), and Kuneba (d) stations at SPI's 3-month (bar-plots) and 12-month (line-plots) time scales. Blue colors represent positive values, and red represents negative values.

Similarly, extreme drought was quantified by the SPEI 3-month time scale at Argoba (-2.60 for 2009), Dubti (-2.20 for 2015), Gewane (-3.33 for 2015), and Kuneba (-3.08 for 2009) stations. Extreme drought quantified by the SPEI 12-month time scale at the same stations was -2.27, -2.01, -2.21, and -5.35, computed for 2016, 2008, 2015, 2011, and 2008, respectively (Figure 4).

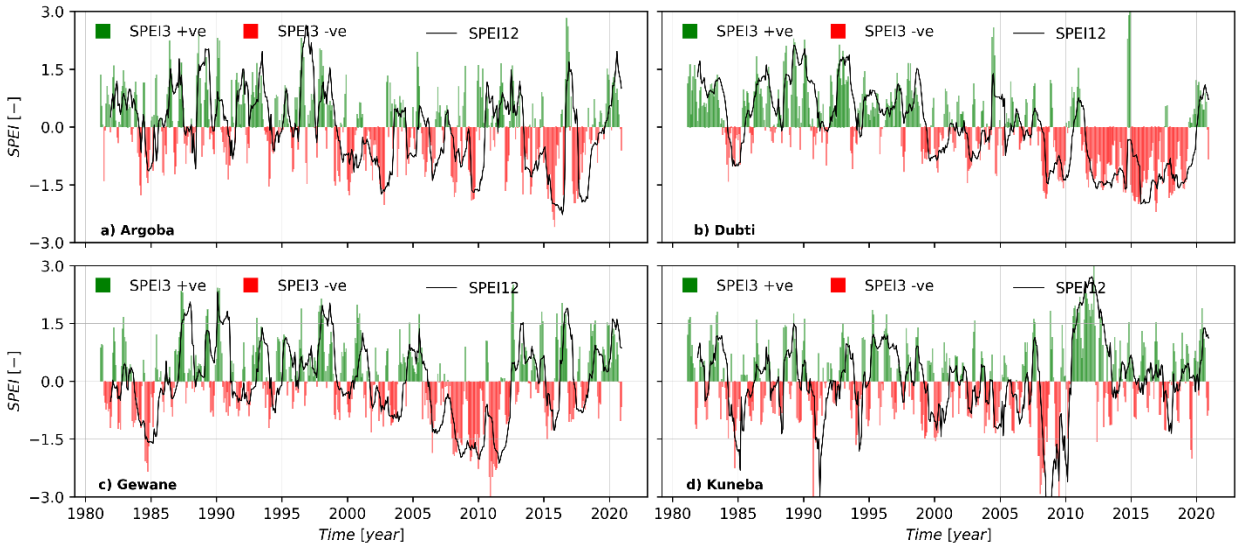

Figure 4| Time series plot for Argoba (a), Dubti (b), Gewane (c), and Kuneba (d) stations at SPEI's 3-month (bar-plots) and 12-month (line-plots) time scales. Green colors represent positive values, and red represents negative values.

3.2 SPI and SPEI drought indices

Table 3 presents the drought frequency and intensity for SPI and SPEI at 3-month and 12-month time scales. The spatial averaged time series findings indicated that SPEI identifies drought more frequently than SPI at both medium and longer scales. For example, the drought frequency identified by SPEI at 3-month and 12-month scales is 17.8% and 16.0%, respectively. At the same time, the drought frequency identified by SPI at the 3-month and 12-month scales is 16.6% and 13.2%, respectively. The drought intensity quantified by SPI 3-month time scale at Argoba, Dubti, Gewane, and Kuneba stations were -1.6%, -1.2%, -1.4%, and -1.5%, respectively. Whereas the drought intensity quantified by SPI, 12-month time scale at the same stations were -2.0%, -1.6%, -1.4%, and -1.8%, respectively. Similarly, the drought intensity quantified by the SPEI 3-month time scale at Argoba, Dubti, Gewane, and Kuneba stations was -1.5%, -1.5%, -1.5%, and -1.4%, respectively. At the same time, the drought intensity quantified by the SPEI 12-month time scale at the same stations were -1.5%, -1.4%, -1.5%, and -1.8%, respectively (Table 3).

The station drought frequency analysis indicated frequent droughts over the study area with varying severity during the last 40 years. For example, the drought frequency identified by the SPI 3-month time scale at Argoba, Dubti, Gewane, and Kuneba stations was 15.9%, 14.0%, 18.4%, and 15.1%, respectively. At the same time, the frequency of drought identified by the SPI 12-month time scale at the same station was 13.7%, 18.8%, 16.5%, and 13.2%, respectively. Similarly, the drought frequency identified by SPEI

at a 3-month time scale at Argoba, Dubti, Gewane, and Kuneba stations were 16.8%, 17.2%, 14.0%, and 16.1%, respectively. At the same time, the drought frequency identified by the SPEI 12-month time scale at the stations mentioned above were 16.7%, 20.2%, 16.5%, and 13.7%, respectively (Table 3).

Table 3| Drought frequency [%] and intensity [%] calculated for SPI and SPEI at 3-month and 12-month time scales.

Station	Frequency [%]				Intensity [%]				Extreme drought months
	SPI 3	SPEI 3	SPI 12	SPEI 12	SPI 3	SPEI 3	SPI 12	SPEI 12	
Argoba	15.9	16.8	13.7	16.7	-1.6	-1.5	-2.0	-1.5	
Dubti	14.0	17.2	18.8	20.7	-1.2	-1.5	-1.6	-1.4	
Gewane	18.4	14.0	16.5	16.5	-1.4	-1.5	-1.5	-1.5	
Kuneba	15.0	16.1	9.4	13.7	-1.5	-1.4	-1.6	-1.8	
Spatial average	16.5	17.8	13.2	16.0	-1.5	-1.4	-1.8	-1.5	

The correlation and regression analysis are used to associate the relationship between SPI and SPEI at 3-month, 6-month, 12-month and 24-moth time scale. For the comparison of both indices, correlation Heatmaps and scatter plotting are presented in supplementary**Error! Reference source not found.**Figures 4 and 5, and statistically evaluated by using the coefficient of determination and correlation coefficient. The SPI and SPEI calculated at different time scales are strongly correlated ($r > 0.7$) at a 0.05 significant level, indicating a fair degree of agreement between the two indices. The regression result indicated that strongest fit has been shown by values of SPI and SPEI at 6-month time scale, with R-squared value of 91.20% of the variation. Moreover, the value of SPI gives closer result with SPEI in the same time scale (Supplementary Figure 5**Error! Reference source not found.**). According to Supplementary Figure 5, the highest value of R-square is 0.912 for SPI and SPEI at 6-month time scale while the lowest is 0.8724 for SPI and SPEI at 24-month time scale.

3.3 Spatial characteristics of drought

The spatial extent of drought frequency, duration, and magnitude was calculated by inverse distance weighted (IDW) interpolation method for SPEI at 3-month and 12-month time scales (Figure 5). The most frequent drought prevailed at Chifra, Gewane, Dalifagi, and Telalak stations, where the drought frequency ranged from 17.3% to 19.9% during the 1981-2020 period for a 3-month time scale. Whereas for the 12-month time scale, the maximum drought frequency prevailed at Semera, Dubti, Elidar, Mille, Chifra, Awura, Bidu, and Melkasedi stations with drought frequency in the range of 18.4% to 21.2% (Figure

5a,b). The drought duration at the 3-month time scale shows that longer duration prevailed at Chifra, Gewane, Telalak, Dubti, Ewa, and Argoba stations with a drought length of 81 to 95 months over the 1981-2020 period. Whereas at a 12-month time scale, the longer drought duration was quantified at Dubti, Awura, Gewane, Mille, Dawe, Semera, and Chifra stations, ranging from 83 to 99 months, respectively (Figure 5 c, d). Drought magnitude showed that more intense drought quantified at Dalifagi, Gewane, Telalak, Chifra, Awura, Ewa, Teru, and Yalo meteorological stations with magnitude in the range of 117.3 to 162.6 for a 3-month time scale. At the longer time scale, more intense drought was calculated at Dalifagi, Gewane, Dubti, Awura, Assaita, Dawe, Mille, and Semera stations with magnitude in the range of 122.6 to 242.7 throughout 1981 to 2020, respectively (Figure 5 e,f).

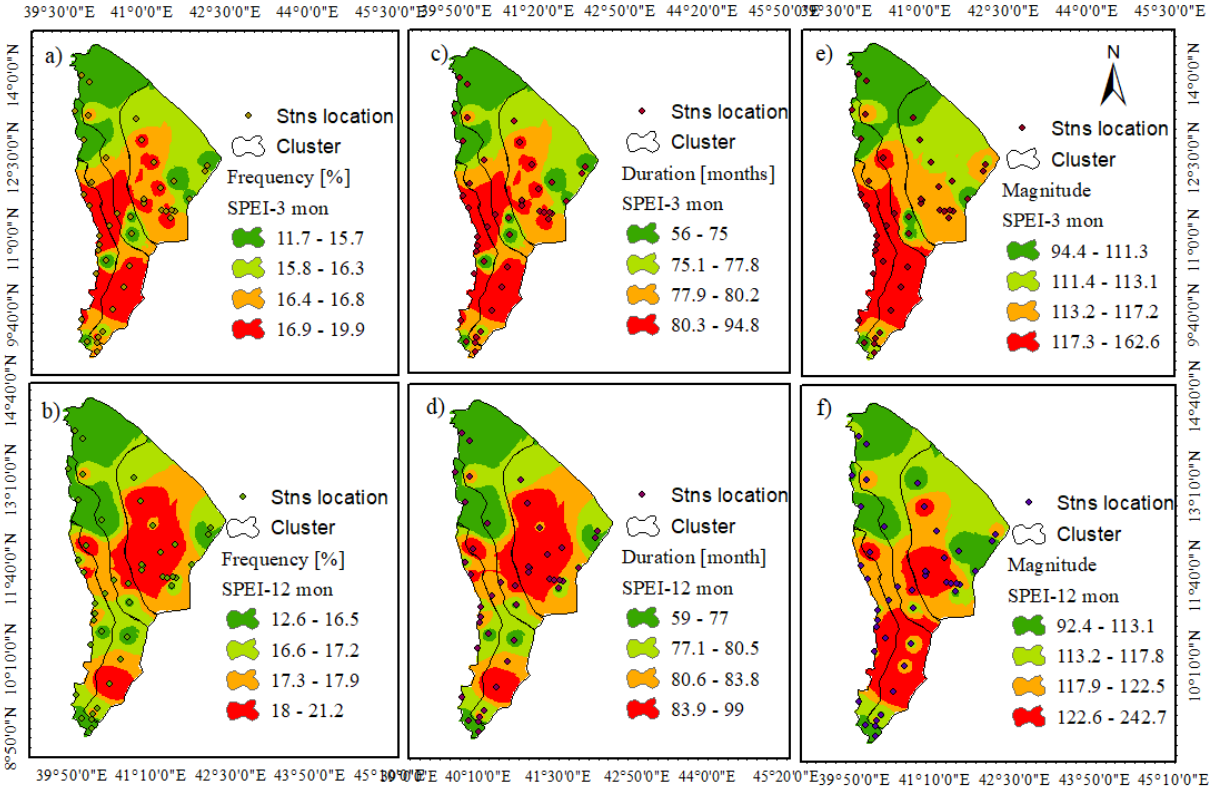

Figure 5| Drought frequency [%] (left panel), duration [months] (middle panel), and magnitude [%] (right panel). The upper row shows the SPEI 3 months, and the lower row shows the SPEI 12-month scale.

Figure 6 presents the number of stations [%] that showed drought during the 1981 to 2020 period for Belg (February to May) and Kiremt (June to July) farming seasons. All 44 meteorological stations showed drought occurrence in 1984 for both seasons. For the 1984, 2008, 2009, and 2015 years, the Belg drought propagated to Kiremt for nearly all the stations **(**Figure 6).

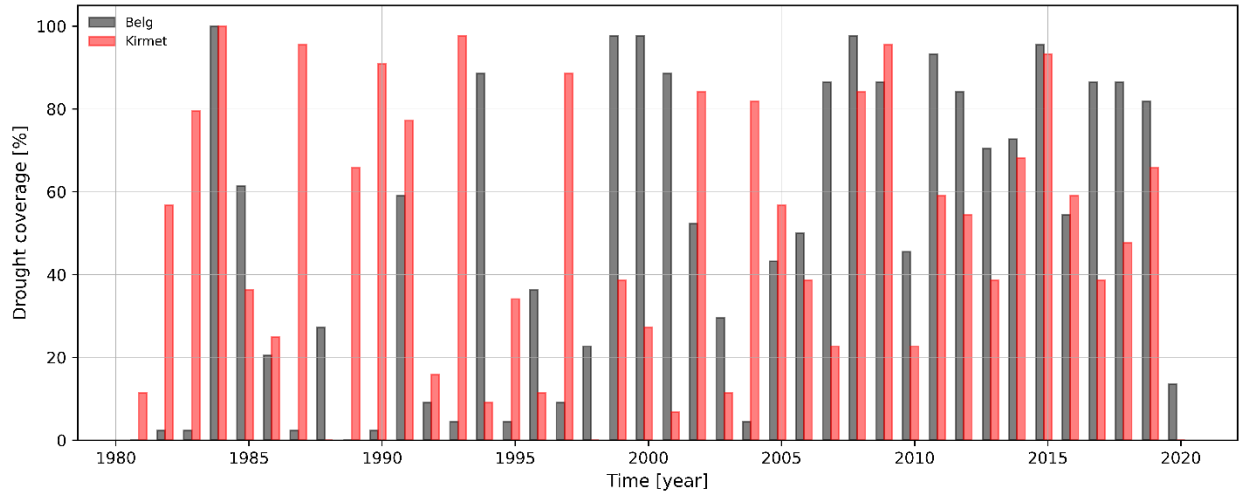

Figure 6| Number of stations [%] that recorded drought during the Belg and Kiremt farming seasons for the 1981-2020 period. Black and red represent drought during Belg and Kiremt seasons, respectively. The most widespread drought coverage prevailed during the Belg cropping season, particularly after 1999 (Figure 6).

Table 4 Presents drought trends and magnitudes throughout 1981-2020 period which shows how drought is severe during Belg and Kiremt cropping season at climate station. The modified MK and Sen's slope Estimator were used to determine trend and magnitude, respectively under the SPEI 4-month time scale. During the Belg crop growing period, 41 stations demonstrated a negative trend. Among the 41 stations, 17 indicated significantly increasing trend toward dryness, with magnitude of in the range -1.25 to -10.0. The strong magnitude was recorded in Dubti, Abala, Gedamaitu, Awash-7 kilo, Semera Afambo, Afdera, Dalifagi, Dawe, Berhaile, Megale, Mille with magnitude of in the range -3.75 to -10.0. Similarly, the drought characteristics during Kiremt crop growing period indicated low significant as compared to Belg crop growing period. Among 44 investigated stations, only 15 stations indicated increasing trend toward dryness, with magnitude ranging from -2.21 to -12.5. The strongest magnitude recorded at Afambo station and have a Sen's slope magnitude estimator of -12.5. The table also shows that there was no significant increasing or decreasing trend at any of the climate stations during Kiremt season. Moreover, the drought indices over the study area revealed no significant trends nearly all of the stations in Kiremt period (Table 4).

Table 4| Drought trend during Belg and Kiremt farming seasons under SPEI-4 month time scale.

No	Stations	Belg				Kiremt			
		Kendall's tau	S'	p-value	Sen's slope	Kendall's tau	S'	p-value	Sen's slope
1	Abala	-0.444	-16	0.0153	-9.5	0.000	0	0.000	3.25
2	Adaitu	0.111	4	0.6265	1.75	0.333	12	0.300	1.25
3	Afambo	-0.444	-16	0.0153	-7.75	-0.333	-12	0.144	-8.25
4	Afdera	-0.444	-16	0.0117	-8.25	-0.167	-6	0.396	-1.75
5	Argoba	-0.278	-10	0.2291	-2.5	-0.111	-4	0.566	-1.75
6	Asara	-0.167	-6	0.3559	-3.75	0.389	14	0.166	4.5
7	Assaita	0.167	6	0.3958	4	0.222	8	0.450	4
8	Awaramelka	-0.056	-2	0.8383	-2	0.500	18	0.070	0.574
9	Awasharba	-0.222	-8	0.3020	-8.5	-0.056	-2	0.838	-0.5
10	Awashsebat	-0.389	-14	0.0166	-4.25	-0.111	-4	0.675	-3
11	Awashsheleko	-0.111	-4	0.5661	-4.25	-0.056	-2	0.838	-4.25
12	Awura	0.000	0	1.0000	-1	0.000	0	0.000	5.75
13	Berhaile	-0.389	-14	0.0097	-4.5	0.056	2	0.882	2.5
14	Bidu	-0.278	-10	0.2291	-3.5	-0.056	-2	0.838	-1.63
15	Bure	-0.389	-14	0.0139	-5.25	0.222	8	0.450	3.5
16	Chifra	-0.167	-6	0.3958	-1	0.056	2	0.854	1
17	Dalifagi	-0.222	-8	0.0256	-4.5	0.389	14	0.214	2.75
18	Dawe	-0.278	-10	0.0289	-4.5	0.056	2	0.838	0.25
19	Ditchoto	-0.333	-12	0.1886	-6.75	-0.056	-2	0.865	0
20	Dobi	-0.111	-4	0.6265	-2.25	0.333	12	0.144	3
21	Dubti	-0.667	-24	0.0414	-10	-0.222	-8	0.288	-3
22	Elidar	-0.278	-10	0.2061	-4.5	0.000	0	0.000	0
23	Elwiha	-0.222	-8	0.4280	-4.75	0.222	8	0.256	6.75
24	Endifo	-0.167	-6	0.3958	-5	0.389	14	0.139	4
25	Erebti	-0.167	-6	0.5403	-3.75	0.444	16	0.089	5.75
26	Ewa	-0.389	-14	0.0126	-5	0.222	8	0.352	4.5
27	Galafi	-0.222	-8	0.2876	-3.5	0.167	6	0.396	3.25
28	Gedamaitu	-0.611	-22	0.0094	-9.5	-0.222	-8	0.239	-1.5
29	Gerjele	-0.278	-10	0.0181	-6.5	0.056	2	0.838	2
30	Gewane	-0.278	-10	0.2888	-3	0.278	10	0.181	4.5
31	Harsis	-0.056	-2	0.8535	-3.25	-0.056	-2	0.854	-0.5
32	Kasagita	-0.389	-14	0.0126	-8.25	0.000	0	0.000	1.5
33	Kuneba	-0.222	-8	0.2389	-1.25	0.111	4	0.614	3.25
34	Logia	-0.111	-4	0.5661	-7.5	0.111	4	0.667	2
35	Manda	-0.278	-10	0.2505	-4.5	0.167	6	0.429	1.25
36	Megale	-0.111	-4	0.0054	-4	0.056	2	0.854	1.75
37	Melkasedi	-0.333	-12	0.0153	-6.25	-0.222	-8	0.302	-1.75
38	Mille	-0.167	-6	0.3958	-3.75	0.278	10	0.289	5.25
39	Semera	-0.333	-12	0.0153	-8.25	-0.111	-4	0.566	-3.25
40	Serdo	-0.389	-14	0.1658	-6.5	-0.222	-8	0.302	-0.75
41	Slisa	-0.278	-10	0.0155	-2.25	-0.167	-6	0.396	-1.25
42	Telalak	-0.167	-6	0.3958	-3	0.167	6	0.396	2.25
43	Teru	-0.167	-6	0.4577	-1.75	0.000	0	0.000	0
44	Yalo	-0.056	-2	0.8651	-0.5	0.000	0	0.000	0.75

3.4 Future drought frequency and magnitude projections

Dubti and Awash meteorological stations are selected to project future drought occurrence over the study area. The two stations are here used as reference climate stations due to the available historical dataset to evaluate historical climate model performance. As indicated in Figure 1, the two stations are located at lower elevation (Dubti station) at Dubti cluster and higher elevation (Awash station) at Awash cluster in the available stations network. Figure 7| Drought frequency [%] at Dubti and Awash stations under RCP 4.5 and 8.5 climate scenarios for the near-term (2006-2040), mid-term (2041-2070), and end of the century (2071-2100).

presents drought frequency at Dubti and Awash stations under RCP 4.5 and 8.5 forcing scenarios. We select the two stations because of better observational data records (>81%) and representativeness of the high (Awash) and low (Dubti) precipitation distribution of the Afar region. The result indicated that more intense drought is likely in both climate-forcing scenarios in the middle and end of the century. For instance, the average change (compared to the baseline period) in drought frequency under RCP4.5 is likely to increase by 2.7% and 8.3% (near future), 8.2% and 33.2% (mid-century), and 11% and 44.8% (end of the century) at Dubti station. Under the same climate forcing, the drought frequency is likely to increase by 12.2% and 10.1% (near future), 35.3% and 53.2% (mid-century), and 33.2% and 30.3% (end of this century) at Awash station. The average change in drought frequency under RCP8.5 forcing scenarios is likely to increase by 2.6% and 2% (near future), 12.9% and 12.8% (mid-century), and 38.7% and 73.2% (end of the century) at Dubti station. For Awash station, the average change in drought frequency is likely to increase by 11.9% and 6.9% (near future), 16.1% and 18.2% (mid-century), and 50.7% and 54.4% (end of the century) as calculated for SPEI 3- and 12-months scale (Figure 7).

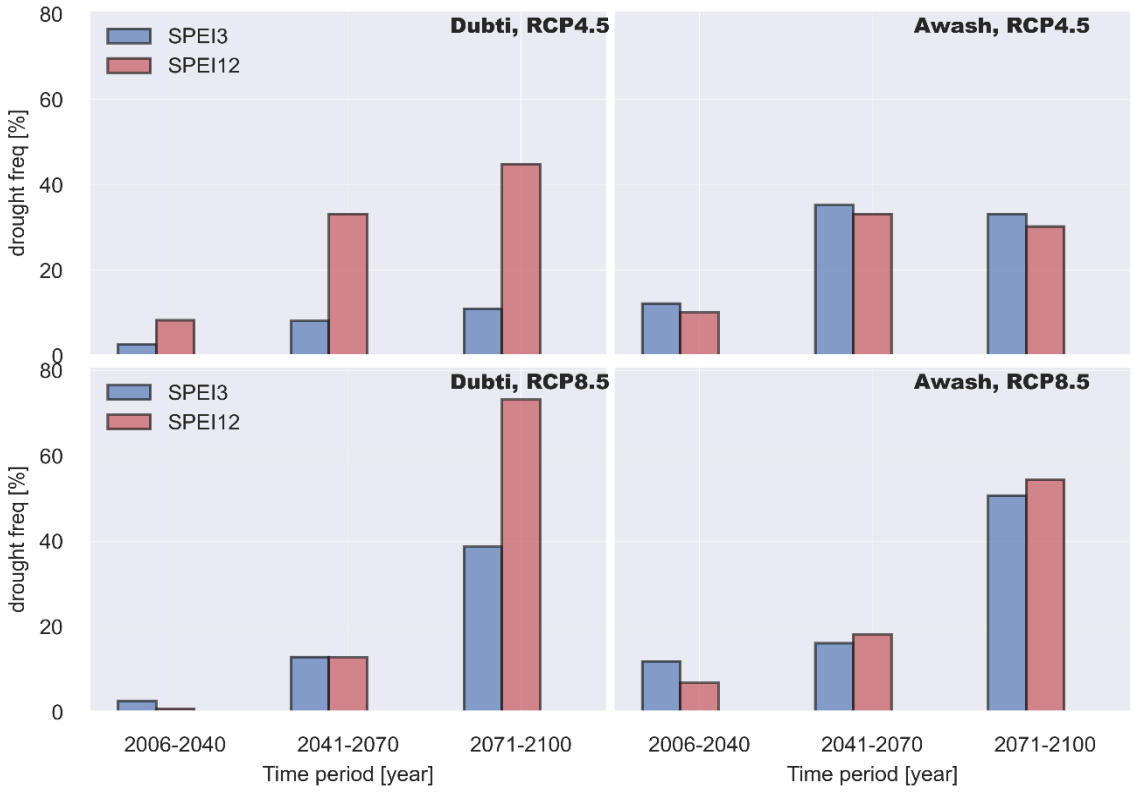

Figure 7| Drought frequency [%] at Dubti and Awash stations under RCP 4.5 and 8.5 climate scenarios for the near-term (2006-2040), mid-term (2041-2070), and end of the century (2071-2100).

As compared to the baseline climatological period (1981-2005), the average change in drought magnitude at Dubti station under RCP4.5 scenarios is likely to increase by 3.3% and 16.4% (near-century, 11.9% and 81.0% (mid-century), and 16.9% and 124.1% (end-century). Similarly, the average change in drought magnitude at Awash station is likely to increase by 14.0% and 11.4% (near-century), 43.5% and 46.1% (mid-century), and 36.8% and 39.2% (end-century). Under RCP8.5 scenarios, the average change in drought magnitude is likely to increase by 3.1% and 2% (near future), 17.1% and 41.0% (mid-century), and 68.4% and 252.2% (end of the century) at Dubti station. Likewise, the average change in drought magnitude at Awash station is likely to increase by 16.3% and 8.8% (near future), 22.8% and 25.6% (mid-century), and 74.0% and 93.6% (end-century) (Figure 8).

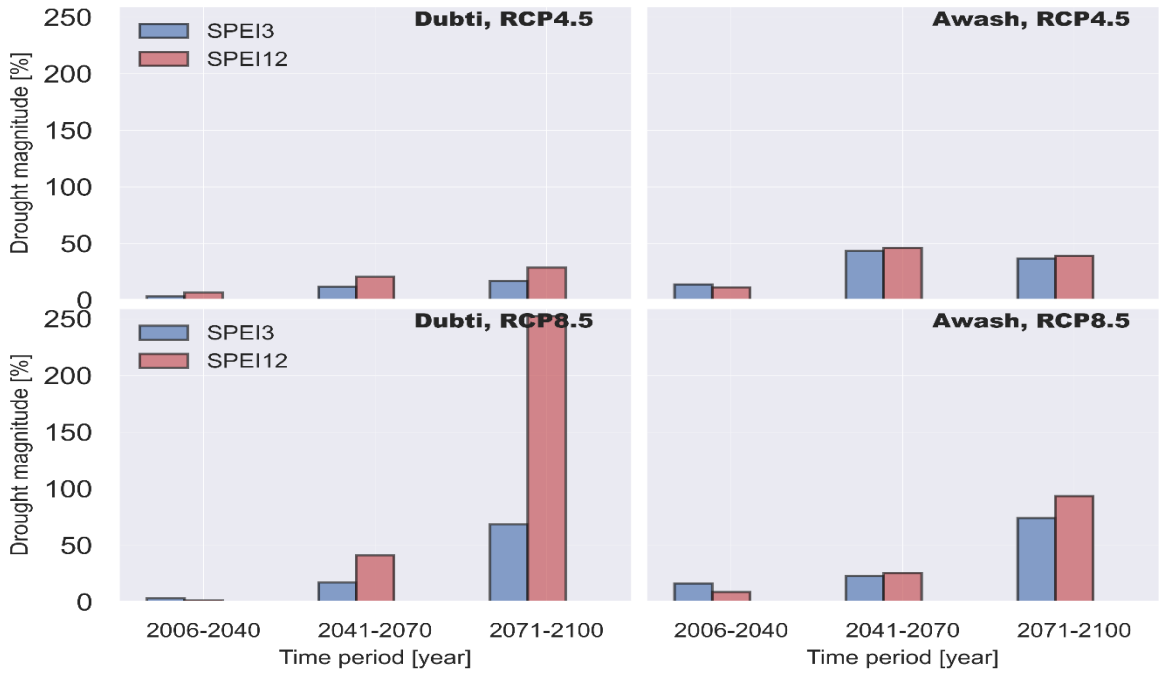

Figure 8| Drought magnitude [%] at Dubti and Awash stations under RCP 4.5 and 8.5 climate scenarios for the near-term (2006-2040), mid-term (2041-2070), and end of the century (2071-2100).

3.5 Association between drought and crop yield

The annual average productivity of major cereal crops (in quintal per hectare - qt/ha) over the entire Afar region for meher harvesting season was compared to the drought indices calculated by SPI and SPEI at 4-month time scale (June-September) period to evaluate the impact of drought on yield (Figure 9). We selected the medium time scale (4 months) to calculate drought as this time scale is suitable for describing agricultural droughts based on soil moisture availability, which provides a seasonal moisture estimation (WMO, 1987). The findings indicate that, in general, there is a significant increasing trend in crop yield over the region during the period 1994 to 2012 (Figure 9a). The correlation between drought indices and yield anomaly showed a strong positive correlation between calculated drought indices and yield anomaly (r^2 = 0.56 and 0.18 for SPI and SPEI, respectively (Figure 9b,c). Other non-climatic factors, such as improved seed varieties, crop management options, etc., are not considered in our analysis yet explain year-to-year yield variabilities.

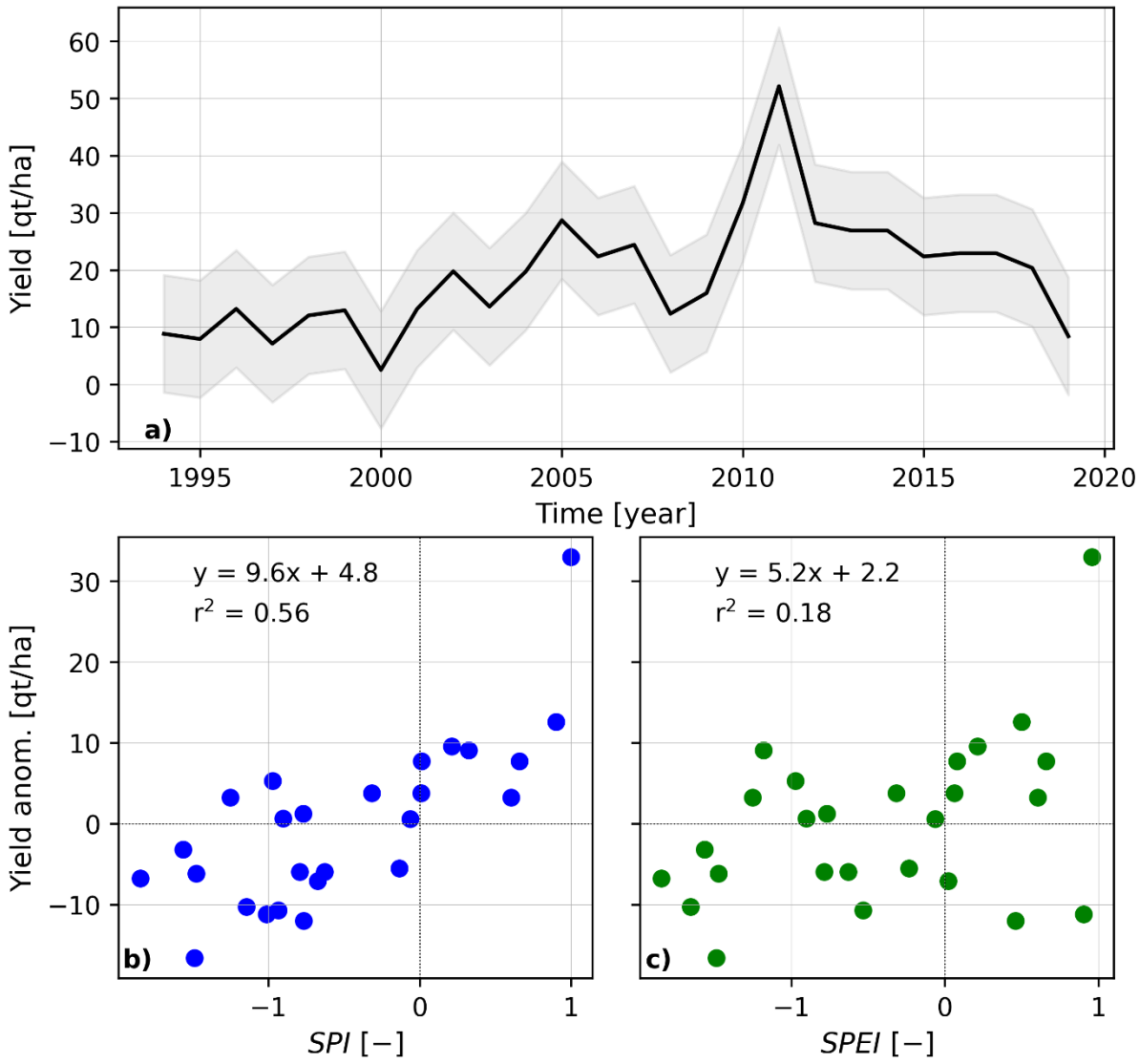

Figure 9| Observed average crop yield during Kiremt cropping season over 1994 -2019 (a), yield anomalies as a function of drought indices: SPI (b) and SPEI (C).

4 DISCUSSION

Ethiopia is a sub-Saharan African country located in the Horn of Africa. It is mainly vulnerable to drought, yet some parts of the nation are more vulnerable than others. Studies show that Ethiopia has experienced drought every two to three years, particularly in the northern and northeastern regions of the country (Mera, 2018). As reported by WFP, the 2015 drought was the worst in the past 30 years, exacerbating food insecurity in the nation (WFP, 2016). The Afar regional state is among Ethiopia's drought-prone areas, frequently and severely affected by recent drought. Recently, the region was severely affected by drought in 2005, 2009, and 2015, in which livelihoods were adversely affected (Ashenif, 2016).

Several researchers in Ethiopia have conducted meteorological drought studies, mainly examining historical data. Very few studies have highlighted future drought evolutions considering the ongoing climate change. The studies also considered Ethiopia, while limited ones focused on the Afar regional state. Furthermore, most of these studies evaluated drought using SPI, and only a few studies implemented SPEI based on satellite rainfall and temperature estimates. For instance, Viste et al. (2013) examined meteorological drought in Ethiopia using SPI from 1970 to 2011 and using data from the Global Precipitation Climatology Project. According to their study, on a national level, 2009 was identified as the second driest year, following 1984. In the 1984 drought over the Afar region, all districts were affected by the failure of seasonal rain (received only 18% of its expected mean annual precipitation) (Viste et al., 2013). Ashenif (2016) examined drought over the Afar region using SPI. The results showed extreme drought in the region in 2005, 2009, 2011, and 2015. In our study, we used >70% of the available climatic stations in the Afar region and deployed downscaled ERA5 reanalysis to fill the gaps in the observations. In addition to the SPI, we evaluated SPEI to consider the region's ongoing global warming and drought. The calculated drought indices are also associated with crop yield to understand the impact on the agricultural sector.

The temporal assessment of meteorological drought revealed that severe and extreme drought prevailed during the last 40-year period (1981-2020). The drought characteristics of both SPI and SPEI were consistent at different time scales. They well captured the historically known droughts during the last 40 years, particularly the more severe and extreme ones during the last 20 years. For example, the years 1984, 2008, 2009, and 2015 were considered to be the driest years across nearly all locations with varying levels of severity (Viste et al., 2013; Eze et al., 2022). Drought occurrences before 1970 were at least once every ten years; they have become more frequent and recently occurred every two or three years with varying severity (Gebrehiwot et al., 2011).

The spatial pattern of drought events at the 3-month time scale during the 1981-2020 period across the study area showed frequent drought prevailed with varying severity. The most severe and recurrent drought was recorded in Afar's southern and southwestern parts, particularly in the Gewane and Awash clusters under a medium-range time scale and in a few areas at the Dubti cluster, respectively. Under a longer time-scale, the most intense and frequent drought was recorded at the Dubti cluster (Figure 5a-f).

Our analysis shows that drought frequency and magnitude will likely increase. For representative stations, drought frequency is projected to increase in the near term (~10%), mid-century (~20%), and end of the

century (>40%) (Figure 7). Similarly, drought magnitudes will also increase in the future compared to the present due to the ongoing climate forcing – increased temperatures and increased drying (Aiguo et al., 2004) (Figure 8). Studies have reported that increased global mean temperatures (Trenberth, 2005) may trigger more evapotranspiration and, thus, surface drying, thereby increasing drought intensity (Orke & Li, 2022).

There is a difference in the variance explained in yield by SPI and SPEI. This is resulted, for example, while the SPEI defined more drought as severe and moderate drought with long duration and increasing intensity, SPI determined more extreme drought than those detected by SPEI. Our findings show that crop yield losses (~3-17 qt/ha compared to the mean yield) in 1994-1995, 1999-2000, 2008-2009, and 2019 coincided with severe droughts. Overall, crop yield is strongly associated with calculated drought indices (r^2 of 0.56 for SPI and 0.18 for SPEI) (Figure 9). Moreover, it is noted that Ethiopian agriculture is mainly (>95%) rain-fed agricultural system (Minda et al., 2018). For example, a catastrophic crop loss was observed during the 2015 drought in the Tigray region (Eze et al., 2022). Reduced rainfall and increased evapotranspiration enhance drought occurrence, reducing soil moisture and the consequence impact of crop failures during the crop growing period. Alternative measures such as rainwater harvesting, supplementary irrigation practices, and drought-resistant crop varieties can be suggested to mitigate the recurrent drought impacts in the agricultural sector in the pastoralist region. Drought monitoring and early warning systems can be established and applied (WMO, 2006).

5 CONCLUSIONS

This study examined meteorological drought affecting agricultural productivity in the Afar region, northeast Ethiopia. It is mainly a pastoralist region and is among the frequently drought-affected areas in the country. Therefore, we evaluated the occurrence of meteorological drought using the present and future climate datasets. We also examined the relationship between drought and crop yield. To this end, we deployed 44 surface climatic stations in the Afar regional state to obtain daily precipitation and minimum and maximum temperature data. This data is evaluated for quality, and the missing records are filled out from the CHRIP dataset. To project the future drought, we used regionally downscaled models of the CMIP5 product. The data is corrected for biases. We systematically clustered the study area into four homogenous precipitations and calculated the standardized precipitation and evapotranspiration meteorological drought indices for temporal and spatial drought evaluation. The regional average cereal yield dataset correlates the drought estimates calculated by the indices to evaluate drought impact.

Therefore, our first research question was formulated as to how the spatiotemporal variation of drought has been characterized during the last 40 years. Our result shows a frequent occurrence of drought with varying degrees of severity. The years 1984, 2008, 2009, and 2015 are the driest years across all the meteorological stations. The most frequent drought was exhibited in the region's central, western, and southern parts, while the most intense drought prevailed over the Agroba cluster. Our second research question was related to quantifying the expected changes in drought magnitude and frequency in the coming decade compared to the base period. Our findings show that the average change in projected drought indicates more frequent and intense droughts will likely increase in the middle and end of the century than in the reference period. Our third research question was to analyze the association between meteorological drought and rain-fed cereal crop productivity. In this regard, our findings show that the annual yield variation explained 56% and 18% for the Meher (Kirment) harvesting season quantified jointly in the variation of SPI and SPEI, respectively.

Data and code availability

CHRIP data is available at https://data.chc.ucsb.edu/products/CHIRP/daily/netcdf/. AgERA5 data is available at https://cds.climate.copernicus.eu/cdsapp#!/dataset/sis-agrometeorological-indicators?tab=overview. CMIP5 datasets: https://cordex.org/data-access/. CDT is an open source and can be accessed here: https://github.com/rijaf-iri/CDT. Python codes developed to analyze the data are available upon request.

Authors' contributions

T.B, A.K, T.T.M designed the study; T.B, T.T.M analyzed data and drafted the manuscript; T.T.M, A.K commented and edited the manuscript and supervised the study. All the authors read and approved the final version.

Acknowledgement

The first author's study at Arba Minch University has been supported by EMI. The EMI support has been acknowledged. This research is partly funded by the Water Resources Research Center, Arba Minch University. The Ethiopian Meteorology Institute (EMI) has provided station observations free of cost.

REFERENCE

Aiguo, D., Kevin, E. T., & Taotao, Q. (2004). A Global Dataset of Palmer Drought Severity Index for 1870 – 2002 : Relationship with Soil Moisture and Effects of Surface Warming. *Journal of Hydrometeorology*, *5*(6), 1117–1130.

Alamgir, M., Shahid, S., Hazarika, M. K., & Nashrrullah, S. (2015). *ANALYSIS OF METEOROLOGICAL DROUGHT PATTERN DURING DIFFERENT*. 1–13. https://doi.org/10.1111/jawr.12276

Ashenif, M. A. (2016). *Remote Sensing and GIS Based Drought Vulnerability Assessment: A Case of Afar Regional State, Ethiopia*. Addis Ababa University.

Aytenfisu, A. T. (2024). *Spatiotemporal climate variability and extremes in Middle Awash Afar region Ethiopia : implications to pastoralists and agro-pastoralists food security*. https://doi.org/10.1108/IJCCSM-11-2023-0140

Bachewe, F., Yimer, F., & Minten, B. (2017). *Agricultural price evolution in drought versus non-drought affected areas in Ethiopia*. *88*(January 2014).

Bari, S. H., Rahman, T. U., Hoque, M. A., & Hussain, M. (2016). NU SC. *Atmospheric Research*. https://doi.org/10.1016/j.atmosres.2016.02.008

Begna, T. (2020). *Effects of Drought Stress on Crop Production and Productivity*. *6*(9), 34–43. https://doi.org/https://doi.org/10.20431/2454-6224.0609005

Boslaugh, S. (2012). Pearson Correlation Coefficient. *Encyclopedia of Epidemiology*, *April*. https://doi.org/10.4135/9781412953948.n342

Chai, T., Draxler, R. R., & Prediction, C. (2014). *Root mean square error (RMSE) or mean absolute error (MAE)? – Arguments against avoiding RMSE in the literature*. *2005*, 1247–1250. https://doi.org/10.5194/gmd-7-1247-2014

Cox, A. D. R., Stuart, A., & Stuart, A. (2013). *Biometrika Trust Some Quick Sign Tests for Trend in Location and Dispersion SOME QUICK SIGN TESTS FOR TREND IN LOCATION AND DISPERSION*. *42*(1), 80–95.

Crochemore, L., Ramos, M.-H., & Pappenberger, F. (2016). Bias correcting precipitation forecasts to improve the skill of seasonal streamflow forecasts. *Hydrology and Earth System Sciences*, *20*(9), 3601–3618.

CSA. (1996). *The Federa Democratic Republic of Ethiopia, the Centeral Statistical Agency (CSA) Report on Area and Production of Majr Crops*.

CSA. (2018). *THE FEDERAL DEMOCRATIC REPUBLIC OF ETHIOPIA REPORT ON AREA AND PRODUCTION OF MAJOR*. *I*.

CSA. (2019). *THE FEDERAL DEMOCRATIC REPUBLIC OF ETHIOPIA REPORT ON AREA AND PRODUCTION OF MAJOR*. *I*.

CSA. (2021). *The Federal Democratic Republic of Ethiopia Central Statistical Agency (CSA) Report on Area , Production and Farm Management Practice of Belg Season Crops for Private Peasant Holdings*. *V*, 25.

Dai, A. (2011). Characteristics and trends in various forms of the Palmer Drought Severity Index during 1900–2008. *Journal of Geophysical Research: Atmospheres*, *116*(D12).

Dinku, T., Faniriantsoa, R., Islam, S., Nsengiyumva, G., & Grossi, A. (2022). The Climate Data Tool: Enhancing Climate Services Across Africa. *Frontiers in Climate*, *3*(February). https://doi.org/10.3389/fclim.2021.787519

Dinku, T., Funk, C., Peterson, P., Maidment, R., Tadesse, T., Gadain, H., & Ceccato, P. (2018). Validation of the CHIRPS satellite rainfall estimates over eastern Africa. *Quarterly Journal of the Royal Meteorological Society*, *144*(August), 292–312. https://doi.org/10.1002/qj.3244

Diriba, G. (2020). *Agricultural and Rural Transformation in Ethiopia Obstacles, Triggers and Reform Considerations Policy Working Paper* (Issue January).

EEA. (2021). *Socioeconomic Development in Afar Region* (Issue February).

Ettenmaier, D. E. P. L. (2005). *Twentieth-Century Drought in the Conterminous United States*. 985–1001.

Eze, E., Girma, A., Zenebe, A., Okolo, C. C., Kourouma, J. M., & Negash, E. (2022). Predictors of drought-induced crop yield/losses in two agroecologies of southern Tigray, Northern Ethiopia. *Scientific Reports*, *12*(1), 1–14. https://doi.org/10.1038/s41598-022-09862-x

Feng, H., & Zhang, M. (2015). Global land moisture trends: drier in dry and wetter in wet over land. *Scientific Reports*, *5*(1), 1–6.

FEWSNET. (2016). Illustrating the extent and severity of the 2015 - 16 drought. *Famine Early Warning Systems Network/USAID Southern Africa Special Report*, 1–8.

Florida, S. (2021). *Evaluation of Regional Climate Models (RCMs) Using Precipitation and Temperature-Based Climatic Indices : A Case*.

Funk, C., Peterson, P., Landsfeld, M., Pedreros, D., Verdin, J., Shukla, S., Husak, G., Rowland, J., Harrison, L., Hoell, A., & Michaelsen, J. (2015). The climate hazards infrared precipitation with stations - A new environmental record for monitoring extremes. *Scientific Data*, *2*(December). https://doi.org/10.1038/sdata.2015.66

Gebrehiwot, T., Van der Veen, A., & Maathuis, B. (2011). Spatial and temporal assessment of drought in the Northern highlands of Ethiopia. *International Journal of Applied Earth Observation and Geoinformation*, *13*(3), 309–321.

Gerber, N., & Mirzabaev, A. (2019). Benefits of Action and Costs of Inaction: Drought Mitigation and Preparedness—A Literature Review *. *Drought and Water Crises*, *1*, 95–124. https://doi.org/10.1201/b22009-7

Gleixner, S., Demissie, T., & Diro, G. T. (2020). Did ERA5 improve temperature and precipitation reanalysis over East Africa? *Atmosphere*, *11*(9), 996.

Gummadi, S., Rao, K. P. C., Seid, J., Legesse, G., Kadiyala, M. D. M., Takele, R., Amede, T., & Whitbread, A. (2018). Spatio-temporal variability and trends of precipitation and extreme rainfall events in Ethiopia in 1980–2010. *Theoretical and Applied Climatology*, *134*(3–4), 1315–1328. https://doi.org/10.1007/s00704-017-2340-1

Guttman, N. B. (1999). Accepting the standardized precipitation index: a calculation algorithm 1. *JAWRA Journal of the American Water Resources Association*, *35*(2), 311–322.

Haile, G. G., Tang, Q., Hosseini-Moghari, S. M., Liu, X., Gebremicael, T. G., Leng, G., Kebede, A., Xu, X., & Yun, X. (2020). Projected Impacts of Climate Change on Drought Patterns Over East Africa. In *Earth's Future* (Vol. 8, Issue 7). https://doi.org/10.1029/2020EF001502

Hamed, K. H., & Rao, A. R. (1998). *A modified Mann-Kendall trend test for autocorrelated data*. *204*, 182–196.

Hargreaves, G. H., & Allen, R. G. (2003). History and Evaluation of Hargreaves Evapotranspiration Equation. *Journal of Irrigation and Drainage Engineering*, *129*(1), 53–63. https://doi.org/10.1061/(asce)0733-9437(2003)129:1(53)

Hirsch, R. M. (1981). *TECHNIQUES OF TREND ANALYSIS FOR MONTHLY WATER-QUALITY DATA*. *18*(June).

Lobell, D. B., & Asner, G. P. (2003). Climate and Management in U . S . Agricultural Yields. *Science*, *299*(February), 1032. https://doi.org/10.1126/science.1078475

Mann, H. B. (1945). Non-Parametric Test Against Trend. *Econometrica*, *13*(3), 245–259. http://www.jstor.org/stable/1907187

Masih, I., Maskey, S., Mussá, F. E. F., & Trambauer, P. (2014). A review of droughts on the African continent: A geospatial and long-term perspective. *Hydrology and Earth System Sciences*, *18*(9), 3635–3649. https://doi.org/10.5194/hess-18-3635-2014

McKee, T. B., Doesken, N. J., & Kleist, J. (1993). The relationship of drought frequency and duration to time scales. *Proceedings of the 8th Conference on Applied Climatology*, *17*(22), 179–183.

Mera, G. A. (2018). Drought and its impacts in Ethiopia. *Weather and Climate Extremes*, *22*, 24–35.

Minda, T. T., Molen, M. K. Van Der, Struik, P. C., Combe, M., Jiménez, P. A., Khan, M. S., & Arellano, J. V. De. (2018). The combined e ff ect of elevation and meteorology on potato crop dynamics : a 10-year study in the Gamo Highlands , Ethiopia. *Agricultural and Forest Meteorology*, *262*(April), 166–177. https://doi.org/10.1016/j.agrformet.2018.07.009

Mohammed, S., Alsafadi, K., Enaruvbe, G. O., & Bashir, B. (2022). Assessing the impacts of agricultural drought (SPI / SPEI) on maize and wheat yields across Hungary. *Scientific Reports*, 1–19. https://doi.org/10.1038/s41598-022-12799-w

Mohammed, Y., Yimer, F., Tadesse, M., & Tesfaye, K. (2018). V. *International Journal of Climate Change Strategies and Management*, *10*(1), 142–160. https://doi.org/10.1108/IJCCSM-12-2016-0179

Nanjundan, S., Sankaran, S., Arjun, C. R., & Anand, G. P. (2019). *Identifying the number of clusters for K-Means: A hypersphere density based approach*.

Nsengiyumva, G., Dinku, T., Cousin, R., Khomyakov, I., Vadillo, A., Faniriantsoa, R., & Grossi, A. (2021). Transforming access to and use of climate information products derived from remote sensing and in situ observations. *Remote Sensing*, *13*(22). https://doi.org/10.3390/rs13224721

Orke, Y. A., & Li, M. (2022). *Impact of Climate Change on Hydrometeorology and Droughts in the Bilate Watershed , Ethiopia*. 1–31.

Park, C., Byun, H., Deo, R., & Lee, B. (2015). Drought prediction till 2100 under RCP 8 . 5 climate change scenarios for Korea. *Journal of Hydrology*, *526*, 221–230. https://doi.org/10.1016/j.jhydrol.2014.10.043

Patakamuri, S. K., & Brien, N. O. (2021). *Modifiedmk : Modified Mann Kendall Trend Tests Package ' modifiedmk .' January*. https://doi.org/10.1023/B

Potopova, V., Boroneanţ, C., Boincean, B., & Soukup, J. (2016). Impact of agricultural drought on main crop yields in the Republic of Moldova. *International Journal of Climatology*, *36*(4), 2063–2082.

Quiring, S. M. (2009). Monitoring drought: An evaluation of meteorological drought indices. *Geography Compass*, *3*(1), 64–88. https://doi.org/10.1111/j.1749-8198.2008.00207.x

Reath, J., Dong, J., & Wang, M. (2018). *Improved parameter estimation of the log-logistic distribution with applications distribution with applications*. *December 2017*. https://doi.org/10.1007/s00180-017-0738-y

Riahi, K., Rao, S., Krey, V., Cho, C., Chirkov, V., Fischer, G., Kindermann, G., Nakicenovic, N., & Rafaj, P. (2011). RCP 8.5—A scenario of comparatively high greenhouse gas emissions. *Climatic Change*, *109*(1), 33–57. https://doi.org/10.1007/s10584-011-0149-y

Saravi, M. M., Safdari, A. A., & Malekian, A. (2009). *Intensity-Duration-Frequency and spatial analysis of droughts using the Standardized Precipitation Index*. *January*, 1347–1383.

Sen, P. K. (1968). Estimates of the Regression Coefficient Based on Kendall's Tau. *Journal of the American Statistical Association*, *63*(324), 1379–1389. https://doi.org/10.1080/01621459.1968.10480934

Teshome, A., & Zhang, J. (2019). Increase of extreme drought over Ethiopia under climate warming. *Advances in Meteorology*, *2019*. https://doi.org/10.1155/2019/5235429

Thomson, A. M., Calvin, K. V, Smith, S. J., Kyle, G. P., Volke, A., Patel, P., Delgado-Arias, S., Bond-

Lamberty, B., Wise, M. A., & Clarke, L. E. (2011). RCP4. 5: a pathway for stabilization of radiative forcing by 2100. *Climatic Change*, *109*(1), 77–94.

Trenberth, K. E. (2005). The impact of climate change and variability on heavy precipitation, floods, and droughts. *Encyclopedia of Hydrological Sciences*, *17*.

Trenberth, K. E., Dai, A., Van Der Schrier, G., Jones, P. D., Barichivich, J., Briffa, K. R., & Sheffield, J. (2014). Global warming and changes in drought. *Nature Climate Change*, *4*(1), 17–22. https://doi.org/10.1038/nclimate2067

Tumsa, B. C. (2022). Performance assessment of six bias correction methods using observed and RCM data at upper Awash basin, Oromia, Ethiopia. *Journal of Water and Climate Change*, *13*(2), 664–683. https://doi.org/10.2166/wcc.2021.181

Tuo, Y., Duan, Z., Disse, M., & Chiogna, G. (2016). Evaluation of precipitation input for SWAT modeling in Alpine catchment: A case study in the Adige river basin (Italy). *Science of the Total Environment*, *573*(August), 66–82. https://doi.org/10.1016/j.scitotenv.2016.08.034

Umargono, E., Suseno, J. E., & S. K., V. G. (2020). *K-Means Clustering Optimization using the Elbow Method and Early Centroid Determination Based-on Mean and Median*. *474*(Isstec 2019), 234–240. https://doi.org/10.5220/0009908402340240

Vicente-Serrano, S. M., Beguería, S., & López-Moreno, J. I. (2010). A multiscalar drought index sensitive to global warming: the standardized precipitation evapotranspiration index. *Journal of Climate*, *23*(7), 1696–1718.

Vicente-Serrano, S. M., Beguería, S., Lorenzo-Lacruz, J., Camarero, J. J., López-Moreno, J. I., Azorin-Molina, C., Revuelto, J., Morán-Tejeda, E., & Sanchez-Lorenzo, A. (2012). Performance of drought indices for ecological, agricultural, and hydrological applications. *Earth Interactions*, *16*(10). https://doi.org/10.1175/2012EI000434.1

Viste, E., Korecha, D., & Sorteberg, A. (2013). Recent drought and precipitation tendencies in Ethiopia. *Theoretical and Applied Climatology*, *112*(3–4). https://doi.org/10.1007/s00704-012-0746-3

Wakie, T. T., Evangelista, P. H., Jarnevich, C. S., & Laituri, M. (2014). Mapping current and potential distribution of non-native Prosopis juliflora in the Afar region of Ethiopia. *PloS One*, *9*(11), e112854.

Wang, Q., Wu, J., Lei, T., He, B., Wu, Z., Liu, M., Mo, X., Geng, G., Li, X., Zhou, H., & Liu, D. (2014). Temporal-spatial characteristics of severe drought events and their impact on agriculture on a global scale. *Quaternary International*, *349*, 10–21. https://doi.org/10.1016/j.quaint.2014.06.021

Wang, W., & Vrijling, J. K. (2005). Trend and Stationarity Analysis for Stareamflow Processes of Rivers in Western Europe in the 20Th Century. *Europe*, *July*, 8–10.

WFP. (2014). *Climate risk and food security in Ethiopia :*

WFP. (2016). *WFP Ethiopia, Drought Emergency Situation Report #3*. *April*, 1–2.

Wilhite, D. A., & Glantz, M. H. (1985). *Understanding the Drought Phenomenon : The Role of Definitions Understanding the Drought Phenomenon : The Role of Definitions*.

WMO. (1987). Standardized Precipitation Index User Guide. *Journal of Applied Bacteriology*, *63*(3), 197–200.

WMO. (2006). Drought monitoring and early warning : concepts , progress and future challenges. *World Meteorogical Organization*, *1006*, 24. http://www.wamis.org/agm/pubs/brochures/WMO1006e.pdf

Worku, G., Teferi, E., Bantider, A., Dile, Y. T., & Taye, M. T. (2018). Evaluation of regional climate models performance in simulating rainfall climatology of Jemma sub-basin, Upper Blue Nile Basin, Ethiopia. *Dynamics of Atmospheres and Oceans*, *83*, 53–63.

Yue, S., & Wang, C. Y. (2002). *Applicability of prewhitening to eliminate the influence of serial correlation on the Mann-Kendall test*. *38*(6), 1–7.

Yue, S., & Wang, C. Y. (2015). *Applicability of Prewhitening to Eliminate the Influence of Serial Correlation on the Mann-Kendall Test Applicability of prewhitening to eliminate the influence of serial correlation on the Mann-Kendall test*. *December*. https://doi.org/10.1029/2001WR000861

Zollo, A. L., Rianna, G., Mercogliano, P., Tommasi, P., & Comegna, L. (2014). Validation of a simulation chain to assess climate change impact on precipitation induced landslides. In *Landslide Science for a Safer Geoenvironment* (pp. 287–292). Springer.